

A Modified Circle Median Filter Method for Improving Accuracy of Wind Directions Retrieval from SAR Image

Chao Yang^{1,a}, Kaijun Ren², Dongxiang Zhang¹ and Weichen Ni¹,

¹National University of Defense Technology, College of Computer, Changsha 410073, China

²National University of Defense Technology, College of Meteorology and Oceanography, Changsha 410073, China

Abstract. Sea surface wind direction is extremely important for weather forecasts, oil spill monitoring, and so on. Up to now, wind direction retrieval from SAR images is still difficult. There are two conventional methods of retrieving wind directions from SAR images, namely, two-dimensional fast Fourier transform (2D FFT) method and local gradients (LG) method. However, the spectral method works fine on open oceans, and large image areas, such as 20×20km. In this paper, a new method which combines wind direction retrieved from 2D FFT and LG with a modified cycle median filter (CMF) is proposed for improving accuracy of 2D FFT-retrieved wind directions filed. With Comparing different wind direction resolution, the high performance of the new method is validated. With the new method, the resolution of FFT-retrieved wind directions can be improved to 3km×3km

1 Introduction

With high spatial resolution, synthetic aperture radar (SAR) has been one of the most efficient instruments to obtain sea surface wind (SSW) information over large areas. In 1986, Gerling et al.[1] found that the linear structure in the SAR image is related to the wind direction (WD) and extracted the WD from SAR spectra. Besides, marine atmosphere boundary layer (MABL) rolls were also observed in SAR images as linear streaks which is consistent with WD[2]. From then on, the wind streak associated with WD become the main approach to retrieve WD.

The main methods of WD retrieval from SAR including fast Fourier transforms (FFT)[3], wavelet transform (WT)[4], local gradients (LG)[5] and so on. In 1996, Vachon et al. extracted WD through spectral analysis by FFT. But FFT has a weakness for small image, e.g. 10km×10km[6]. In 2003, LG which extracts WD by acquisition of the orthogonal of the most frequent gradient direction is propose by Koch et al. LG overcomes the shortcoming of FFT and works better than FFT on spatial sampling of 10km×10km, even 1km × 1km. The WD from a SAR by FFT or LG exist 180°ambiguity, but it can be removed referencing to weather model output, Doppler shift or land shadows[7, 8].

When retrieving WDs from a SAR image, the SAR image is divided into a set of wind vector cells (WVCs). The direction at each WVC is extracted by FFT or LG. However, there are some isolated impulses in WDs because of noise. The essence different of FFT and LG is that they represent information from frequency domain and spatial domain respectively. In this way, considering combining the two information is meaningful. The cycle

median filter (CMF) technique is frequently used for ambiguity removal in wind vector retrieval from scattermetter[9, 10]. CMF select a wind vector that is the closest vector to the true wind out of a set of ambiguous wind vectors at each WVC[9]. In this way, CMF can be used to improve accuracy of FFT-retrieved WDs by combining LG-retrieved WDs from a SAR image.

In this study, we use a modified CMF to improve FFT-retrieved WDs accuracy in a SAR image by combining LG-retrieved WDs that represent the direction from spatial domain. In addition, the method is tested in different WDs resolution with WD from National Data Buoy Center (NDBC).

The remaining sections are organized as follows. In section 2, the data used in this study are introduced. In section 3, our method is described in detail. The performance of the method is tested in different WDs resolution in section 4. Conclusions are given in section 5

2 Data

Sentinel-1 interferometric mode (IW) mode Ground Range Detected (GRD) Vertical-Vertical (VV) polarization SAR images can be downloaded from European Space Agency (ESA) Sentinels Scientific Data Hub with nominal resolution of 20m×22m and pixel spacing of 10m in range and azimuth, respectively. In this study, we concentrate on WDs retrieval from VV-polarized SAR image. Geometric calibrations are carried out by The Sentinel Application Platform 5.0 (SNAP 5.0)[11].

Not all SAR images have wind streaks, so we select two Sentinel-1 IW mode SAR images in our study. Their information is listed in Table 1. Associated with SAR

^a Corresponding author: yangchao16@nudt.edu.cn

Table 1. Information of SAR Images in IW mode.

	Start Time	End Time	Center Lat(N)	Center Lon(E)
1	2017-05-18T14:16:04Z	2017-05-18T14:16:29Z	36.7694	-123.3518
2	2017-05-18T23:35:38Z	2017-05-18T23:36:03Z	24.5454	-82.5721

Table 2. Information of in suit buoy.

Station	Latitude (N)	Longitude (E)	Wind Direction (°)	Time
46012	37.363	-122.881	318	2017-05-18-14-20
plsf1	24.693	-82.773	97	2017-05-18-23-40

images, the in situ National Oceanic and Atmospheric Administration (NOAA) National Data Buoy Center (NDBC) buoys are collected, which are listed in Table 2, including WD at the time.

3 Method

For wind vector retrieval from scatterometer, a modified median filter is used to select a unique wind vector out of a set of ambiguous wind vectors at each WVC. In this study, we regard WDs extracted by FFT and LG as ambiguous WDs.

For a set of data A with length of N and circular data $x_i \in A, 1 \leq i \leq N$, the median y can be expressed as :

$$y = \operatorname{argmin}_{x \in A} \sum_{i=1}^N |x - x_i| \quad (1)$$

Based on (1), a median filter is implemented by constructing a fixed-length data window which is passed over the data and a set of median data is acquired. For a set of data A with length of N , window length is setted as M . At step j , the data in the window is $D_j = \{x_d | j-h \leq d \leq j+h, h = M/2\}$. As in the following, the expression of (1) can be rewritten as:

$$y_i = \operatorname{argmin}_{x \in D_j} \sum_{m=i-h}^{i+h} |x - x_m| \quad (2)$$

In order to imply median filter into SAR image, extending (2) for two-dimensional data is necessary:

$$y_{ij} = \operatorname{argmin}_{x \in D_{ij}} \sum_{m=i-h}^{i+h} \sum_{n=j-h}^{j+h} |x - x_{mn}| \quad (3)$$

where $D_{ij} = \{x_{pq} | i-h \leq p \leq i+h, j-h \leq q \leq j+h, h = M/2\}$ is the data in $M \times M$ window.

To get more accuracy WD filed is to consider the two-dimensional WD filed $W_{ij} = \{x_{ij}^1, x_{ij}^2 | x_{ij} \in D_{ij}\}$, where each grid point (i, j) has two WD value, which are asscoiated with WDs assignd by FFT and LG algorithm. Let F_{ij}, L_{ij} be the set of FFT-retrieved WD and LG-retrieved WD at grid point (i, j) . Thus,

$$W_{ij} = F_{ij} \cup L_{ij} \quad \text{for all } i, j \quad (4)$$

Let F_{ij} be the initial WD filed at (i, j) grid. In this way, expression (3) can be written as:

$$y_{ij} = \operatorname{argmin}_{x \in F_{ij}} \sum_{m=i-h}^{i+h} \sum_{n=j-h}^{j+h} |x - x_{mn}| \quad (5)$$

At the center of the filter window, we can get a set of medians $\{y_{ij}\}$ of each Window. The modified CMF can be written as:

$$z_{mn} = \operatorname{argmin}_{k=\{1,2\}} \sum_{m=i-h}^{i+h} \sum_{n=j-h}^{j+h} |y_{ij} - x_{mn}^k| \quad (6)$$

where $x_{mn}^k \in W_{ij}$, z_{mn} is the new data in $M \times M$ window.

For each window, the purpose is to select the WD that is closest to the median of the window at each grid point in W_{ij} . The z_{mn} is the value from W_{ij} , which is closest to y_{ij} . In this way, we get a new WD filed $Z_{ij}^* = \{z_{mn}\}$. The Z_{ij}^* is used to replace F_{ij} , and the filter selection process continues for each grid point (i, j) to create new Z_{ij}^* . The whole process is repeated to select a new Z_{ij}^* until $Z_{ij}^* = F_{ij}$. In addition, the WDs from LG or FFT have 180° ambiguity, it's essential to remove 180° ambiguity with WD from NDBC for both FFT-retrieved and LG-retrieved direction firstly.

In the WDs filed retrieved by FFT, the isolated impulses often happen because of the noise. For the smoothness and continuity of wind filed, it's useful to

replace isolated impulses with median value directly, but it's statistical-based method. Our method that uses WDs from LG to replace the error directions from FFT is more meaningful. Besides, it's effective to improve the resolution of FFT-retrieved WDs.

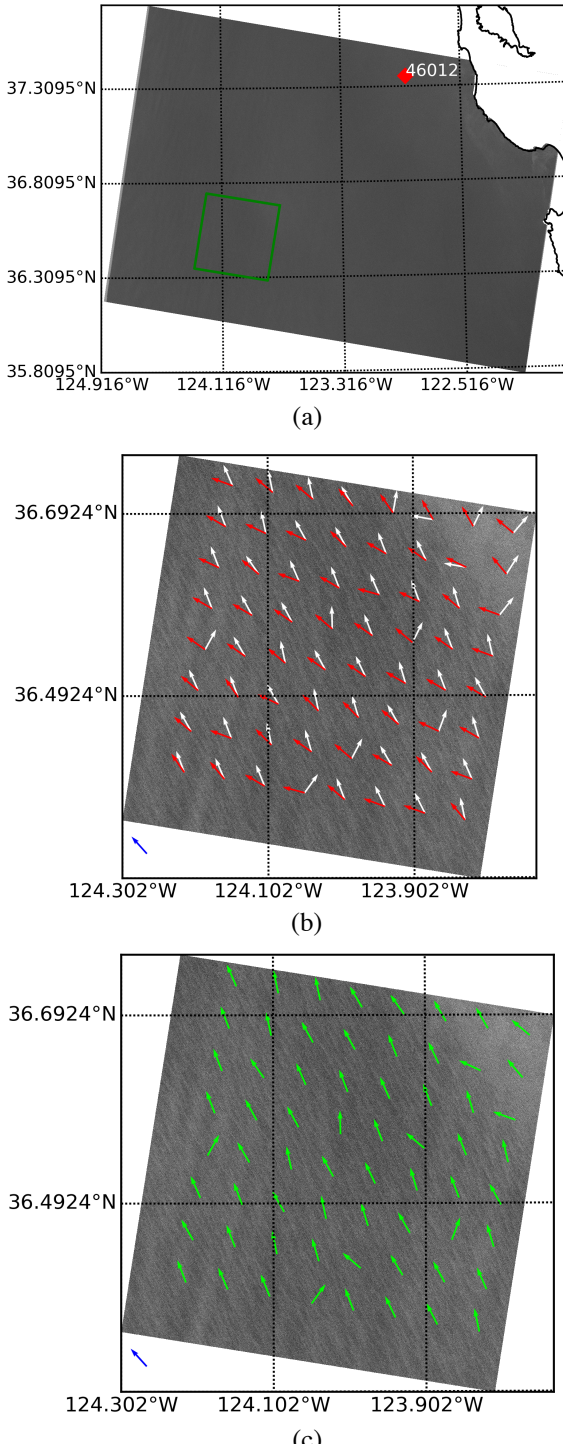


Figure 1. (a) The first SAR image listed in Table 1 in VV polarization with a resolution of 20m. (b) The WDs computed from 10m pixels on a 5km grid by FFT in white color and LG in red color on a 44km by 44km sub-image that is indicated by green box in (a). (c) The WDs from our method on the same sub-image in (b). The blue arrow is the WD from buoy '46012' at the corresponding time.

4 Result

The wind streaks don't appear in all regions of the SAR image, so we find the wind streak patterns in a SAR image and apply FFT and LG to the sub-images at these locations. Besides, 180° ambiguity should be removed by buoy WD after applying FFT and LG. The default window size of our method is 5 and the step that the window passing the data is 2.

The first SAR image listed in Table 1 and acquired by Sentinel-1 IW mode in VV polarization with a resolution of 20m is shown in Figure 1a. The SAR image is shown in grey and the land in the SAR image has been masked out. Besides, associated with the first SAR image, a in situ buoy is marked in red diamond in Figure 1a. On a 44km by 44km sub-image that is indicated by green box in Figure 1a, Figure 1b shows the WDs computed by FFT in white color and LG in red color. WDs are computed from 10m pixels on a 5km grid. The blue arrow (318°) in left-button is the WD from in situ buoy '46012'. The time of WD acquired by buoy is almost consistent with the time of SAR image acquired by Sentinel-1 (error is less than 5 minutes). In addition, the WDs here are in the same coordinate, in which the direction of the northward and eastward wind vector is 0° (or 360°) and 90° respectively.

As illustrated in Figure 1b, the FFT-retrieved WDs are aligned with wind streaks closer than LG-retrieved WDs. That's the reason why we use LG-retrieved WDs to improving accuracy of FFT-retrieved WDs, rather than the other way around. However, there are some isolated impulses in FFT-retrieved WDs because of noise. Figure 1c is same as 1b except the green arrow that is the WDs from our method. It's obvious that our method revises FFT-retrieved WDs at right and top region.

In general, FFT is effective on 20km×20km WVC and the difficulty of extracting WD by FFT is inversely related to the size of WVC[15]. When the wind resolution increase, FFT-retrieved WDs has more and more impulses. As show in Figure 1, our method is effective on 5km×5km. In Figure 2a, the second SAR image listed in Table [tab:1] and a in situ buoy marked in red diamond is shown. Figure 2b is a 37km×33km sub-image indicated by green box in Figure 2a. And the FFT-retrieved WDs in white color and WDs from our method in green color that are acquired on a 4km grid are illustrated in Figure 2b. In Figure 2b, the WDs from our method is almost covered by FFT-retrieved and the steps described in Section 3 just run once. Figure 2c is the same region as Figure 2b, but FFT-retrieved WDs and WDs from our method are both computed on a 3km grid. Note that, there are much more impulses in the FFT-retrieved WDs and we repeat twice the steps. In both 4km-grid and 3km-grid, our method shows a great performance.

CMF is always effective when over 50% of the FFT-retrieved WDs are right. In fact, wavelengths of wind streaks are between 500m and 1500m [5]. When retrieve WDs from smaller region, the wind information can't be acquired from speckle domain of SAR image. Therefore, it's more difficult to retrieve WD when the grids become smaller. In Figure 3, the FFT-retrieved WDs in white color are shown on a 1km grid and the results of our method in green color has changed the mostly wrong directions.

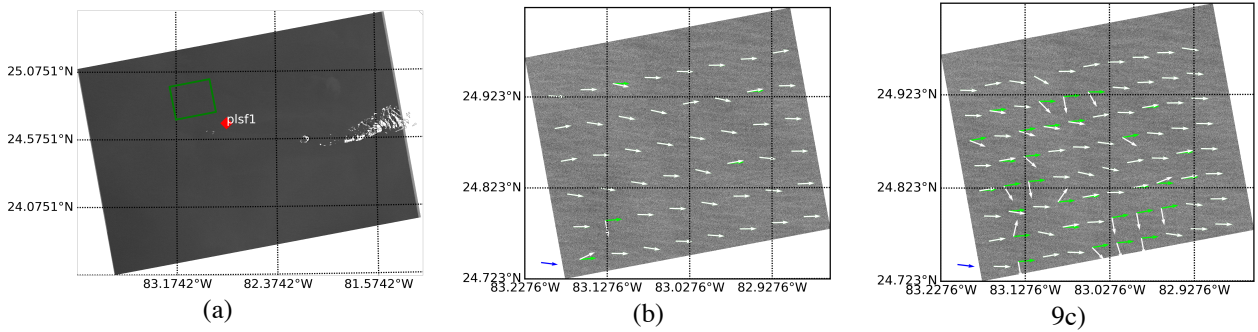


Figure 2. (a) The second SAR image listed in Tabell1 in VV polarization with a resolution of 20m. (b) The WDs computed from 10m pixels on a 4km grid by FFT in white color and our method in green color on a 37km by 33km sub-image that is indicated by green box in (a). (c) The WDs computed on a 3km grid by FFT in white color and our method in green color. The blue arrow is WD from buoy ‘plsf1’ at the corresponding time.

However, impulses are too many to revise. Therefore, the effective of our method is limited by the weakness of FFT.

has to point out is that many WD retrieval methods can be used to replace LG in our method. In future works, we'll test them.

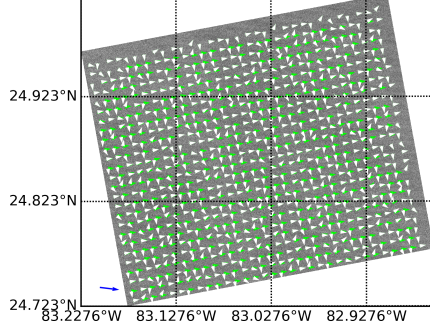


Figure 1. The FFT-retrieved WDs in white color and WDs from our method in green color on a 1km grid on the sub-image in Figure 2b.

5 Conclusion

In this paper, we concentrate on improving accuracy of FFT-retrieved WDs filed retrieved from SAR VV-polarized image by combining the FFT-retrieved directions and LG-retrieved directions. Considering the information of frequency domain and spatial domain, A modified CMF is proposed.

In this work, we modified CMF to select the WDs that is closest to the true WDs from FFT-retrieved WDs and LG-retrieved WDs. Two VV-polarized SAR image from Sentinel-1 IW mode are used to validate our method and the results show the effective. Besides, we analyse the performance of our method in different WDs resolution. Since wavelength of wind streaks is between 500m and 1500m, the resolution of FFT-retrieved WDs is limited. With the WDs resolution increase, it's more and more difficult to retrieve WDs filed using our method, which is caused by the weakness of FFT. However, our method can get higher WDs resolution than that from FFT. Besides, according to our analysis, the new method has high performance in a 3km×3km gird.

In addition, the filter size and step length of our modified CMF are not discussed in this work, and we use filter size of 5 and set length of 2 as default. One thing that

Acknowledgement

This work was supported by the National Natural Science Foundation of China under Grant *****. The Sentinel-1 SAR data and the SNAP 5.0 software are available through the European Space Agency Sentinels Scientific Data Hub and European Space Agency Step Scientific Toolbox Exploitation Platform.

References

1. T W Gerling, *Journal of Geophysical Research: Oceans*, **91**, 2308(1986)
2. W Alpers, B Brümmer, *Journal of Geophysical Research: Oceans*, **99**, 12613–12621(1994)
3. P W Vachon, F W Dobson, *The Global Atmosphere and Ocean System*, **5**, 177–187(1996)
4. Yong Du, Paris W Vachon, *Canadian Journal of Remote Sensing*, **29**, 491–498(2003)
5. W Koch, *IEEE Transactions on Geoscience and Remote Sensing*, **42**, 702–710(2004)
6. Lizhang Zhou, Gang Zheng, Xiaofeng Li, Jingsong Yang, Lin Ren, Peng Chen, Huaguo Zhang, and Xiulin Lou, *Remote Sensing*, **9**(2017)
7. J Horstmann, W Koch, in *Proceedings of IEEE Geoscience and Remote Sensing Symposium (IGARSS)*, 3102–3104(2003)
8. Biao Zhang, William Perrie, Jun A Zhang, Eric W Uhlhorn, and Yijun He, *Journal of Atmospheric and Oceanic Technology*, **31**, 272–286(2014)
9. S J Shaffer, R S Dunbar, and S V Hsiao, *IEEE Transactions on Geoscience and Remote Sensing*, **29**, 167–174(1991)
10. B W Stiles, B D Pollard, and R S Dunbar, *IEEE Transactions on Geoscience and Remote Sensing*, **40**, 79–89(2002)
11. S F James, *Journal of Physics: Conference Series*, **926**, 012004(2017).